Bull. Soc. R. Sci. Liège, 2024, **93**(3), 291–301 *Peer-reviewed conference paper*
doi:10.25518/0037-9565.12365

Probing the X-ray Reprocessing Geometry in High-Mass X-ray Binaries with the *Chandra* High Energy Transmission Grating

Panayiotis TZANAVARIS[1,2,3,*] and Tahir YAQOOB[1,2]

[1] Center for Space Science and Technology, University of Maryland, Baltimore County, 1000 Hilltop Circle, Baltimore MD 21250, USA
[2] Center for Research and Exploration in Space Science and Technology, NASA/Goddard Space Flight Center, Greenbelt, MD 20771, USA
[3] The American Physical Society, Hauppauge, NY 11788, USA
[*] Corresponding author: ptzanava@umbc.edu

Paper presented at the 41st Liège International Astrophysical Colloquium on "The eventful life of massive star multiples," University of Liège (Belgium), 15–19 July 2024.

Abstract

A majority of stars reside in multiple systems, and a majority of massive stars appear in binaries. An important subset goes through an X-ray binary (XRB) phase, but the geometry of their X-ray reprocessing matter that gives rise to prominent spectral features such iron fluorescent X-ray emission remains not well understood. The similarity of XRB spectral features to those of Active Galactic Nuclei (AGN) in the X-rays motivates us to apply similar physical modeling for 10 well-known Galactic High Mass X-ray Binaries (HMXBs) observed with the *Chandra* High Energy Transmission Grating (HETG). Using two different state-of-the art models for X-ray reprocessing, that self-consistently model together Fe Kα fluorescent emission and scattered X-ray continua, we obtain unique insights into the geometry and kinematics of the accretion flow in these systems. Here, we present constraints on the shape as well as distance of the X-ray reprocessor from the accretion disk.

Keywords: X-ray binaries, X-ray spectroscopy, 4U1700–37, 4U1822–371, 4U1908+075, Cen X–3, Cir X–1, Cyg X–1, Cyg X–3, γ Cas, GX 301–2, GX 1+4, Her X–1, LMC X–4, OAO 1657–415, Vela X–1

Résumé

Sondage de la géométrie du retraitement des rayons X par les binaires X de grande masse avec le spectromètre à réseau de transmission à haute énergie sur *Chandra*. La majorité des étoiles résident dans des systèmes multiples, et la majorité des étoiles massives apparaissent dans des binaires. Un sous-ensemble important passe par une phase binaire à rayons X (BRX), mais la géométrie de leur matière retraitant les rayons X, qui génère ainsi des caractéristiques spectrales proéminentes, telles que les raies d'émission de fer fluorescent, reste mal comprise. La similitude des caractéristiques spectrales des BRX avec celles des noyaux galactiques actifs

(NGA) dans les rayons X nous motive à appliquer une modélisation physique similaire pour 10 binaires X de grande masse (BXGM) dans la Galaxie, bien connues et observées avec le spectromètre à réseau de transmission à haute énergie (*High Energy Transmission Grating*) sur *Chandra*. En utilisant deux modèles de pointe différents pour le retraitement des rayons X, qui modélisent de manière cohérente l'émission fluorescente Fe Kα en même temps que les continus des rayons X diffusés, nous obtenons des informations uniques sur la géométrie et la cinématique de l'écoulement d'accrétion dans ces systèmes. Nous présentons ici les contraintes sur la forme ainsi que la distance entre le reprocesseur de rayons X et le disque d'accrétion.

Mots-clés : étoiles binaires à rayons X, spectroscopie de rayons X, 4U1700–37, 4U1822–371, 4U1908+075, Cen X–3, Cir X–1, Cyg X–1, Cyg X–3, γ Cas, GX 301–2, GX 1+4, Her X–1, LMC X–4, OAO 1657–415, Vela X–1

1. Introduction

According to the "canonical" view of systems with Compact Objects (COs), whether Active Galactic Nuclei (AGN) or X-ray Binaries (XRBs), there is a number of prominent spectral components that routinely appear in their X-ray spectra, including an intrinsic power-law continuum, a narrow fluorescent Fe Kα emission line at 6.4 keV and its associated "reflection" (i.e. scattered) continuum, thermal emission from an accretion disk, and a broad Fe Kα emission line with its own associated reflection continuum (Fig. 1). The broad (FWHM $< 10,000\,\mathrm{km\,s^{-1}}$) line arises close to the central object in the strong-gravity regime. Its relativistic broadening can be modeled to measure black hole spin. Instead, the narrow (FWHM $\sim 2,000\,\mathrm{km\,s^{-1}}$) line (henceforth, "narrow line") arises in distant structures, such as the putative AGN torus. In this work we are concerned with the narrow Fe Kα line in Galactic XRBs.

1.1. Narrow Fe Kα emission in Galactic X-ray Binaries

As the narrow line arises far from the central object, whether supermassive black hole, stellar-mass black hole, or neutron star, it constitutes a unique probe of the geometry, dynamics, or element abundances in this distant environment. Its narrow nature means that it is best studied with X-ray gratings, since CCD detectors have FWHM of the order of $\sim 7,000\,\mathrm{km\,s^{-1}}$, compared to the *Chandra* High Energy Transmission Grating's (HETG) $\sim 1,800\,\mathrm{km\,s^{-1}}$ (at ~ 6.4 keV, Canizares et al., 2005). Although emission lines from ionized material are also often detected, we are here concerned with those narrow lines where the centroid is at 6.4 keV, indicating their neutral nature and the relatively cold material that gives rise to them.

In this work, we are motivated by three main questions:

1. Is the *Chandra* HETG capable of resolving these lines in XRBs? Previous work (Torrejón et al., 2010) suggested that the lines remained unresolved.

2. What is the geometry of the reprocessing region? A uniform spherical distribution for all cases has previously been suggested (Torrejón et al., 2010).

3. What is the Fe abundance of the reprocessing matter? A solar abundance would be the simplest expectation.

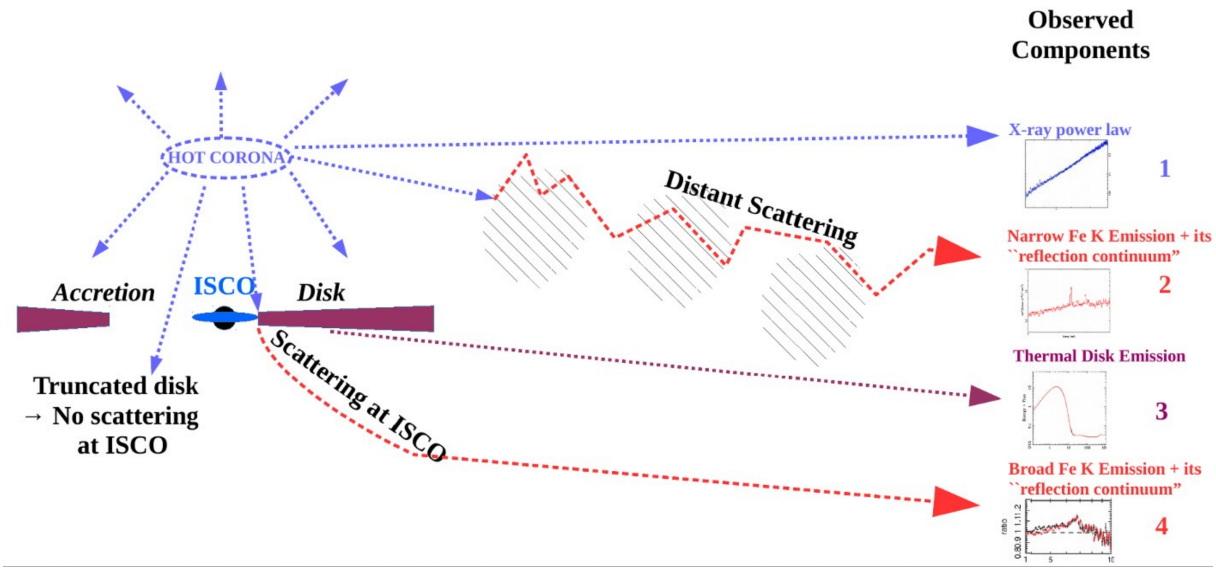

Figure 1: Key components in the canonical X-ray spectral view of COs, both X-ray binaries and AGN. The putative hot corona due to inverse Compton up-scattering of thermal photons at an accretion disk gives rise to the direct X-ray power-law continuum. When this is scattered ("reflected") at the disk and up to the ISCO, it gives rise to relativistic features, including a broad Fe Kα emission line. If instead it is scattered far from the disk and the strong-gravity regime, it gives rise to a narrow Fe Kα line. Fe Kα emission is always associated with its own "reflection" continuum. For illustrative purposes, only disk accretion is shown here. However, six out of the 14 binaries considered in this work are in fact considered wind-fed.

2. Method: Two Physical X-ray Reprocessing Models

For the first time, we use two physically motivated models to fit *Chandra* X-ray spectra of 14 Galactic XRBs. Key characteristics of both models are that the reprocessed, Compton scattered, continuum is produced together with the narrow-line emission, and that the equivalent hydrogen column density, $N_{\rm H}$, is finite, unlike in earlier models such as `pexmon`.

The models are:

1. The uniform spherical matter distribution model of Brightman and Nandra (2011, BN11). This model allows to test directly for our motivating question #2. It also allows for varying the iron abundance, $A_{\rm Fe}$, thus addressing question #3.

2. The decoupled MYTORUS model (Murphy and Yaqoob, 2009; Yaqoob, 2012) which mimics a patchy or clumpy X-ray reflector. This model has a fixed, solar $A_{\rm Fe}$, but models separately the Kα1 and Kα2 components of the line. It also allows for different values for the global (scattered) vs. the line-of-sight (l.o.s.) $N_{\rm H}$ (Fig. 2). It is important to stress that, in spite of the name, this MYTORUS setup *does not, in fact, model a torus* but a patchy distribution of matter or clouds (see Yaqoob (2012) for several possible MYTORUS setups).

3. Sample

The sample (Table 1) used in this work comprises 56 individual HETG observations for 14 Galactic XRBs. Out of these, 10 objects (36 observations) are High-Mass XRBs (HMXBs). However, the results are not significantly different for high- vs. low-mass systems (LMXBs), nor for disk- vs. wind-fed ones, and are thus presented without distinction. The fitting band was 2.4–8.0 keV and Fe K emission was detected in all systems, *except* for seven out of 15 observations of Cyg X–1, as well as all observations of Cir X–1. The upper bound of the fitting band was dictated by the fact that detector sensitivity and effective area fall off sharply above this energy. The lower bound was chosen due to the fact that many spectra showed complex soft X-ray emission. As the ionized material responsible for this is disticnt from that producing the neutral Fe Kα line, and modeling these complex features can complicate considerably the spectral fitting stability without significantly affecting the results we are focusing on, we empirically established the lower bound of 2.4 keV. The data were reduced and fitted with XSPEC 12.8.1g (Arnaud, 1996) as explained in detail in Tzanavaris and Yaqoob (2018), who also show all fitting results both in table and individual plot form.

4. Results

We now return to our motivating questions and how these are addressed by our fitting results. We discuss each question separately below, highlighting some key findings. For the full results and details, the interested reader should turn to Tzanavaris and Yaqoob (2018).

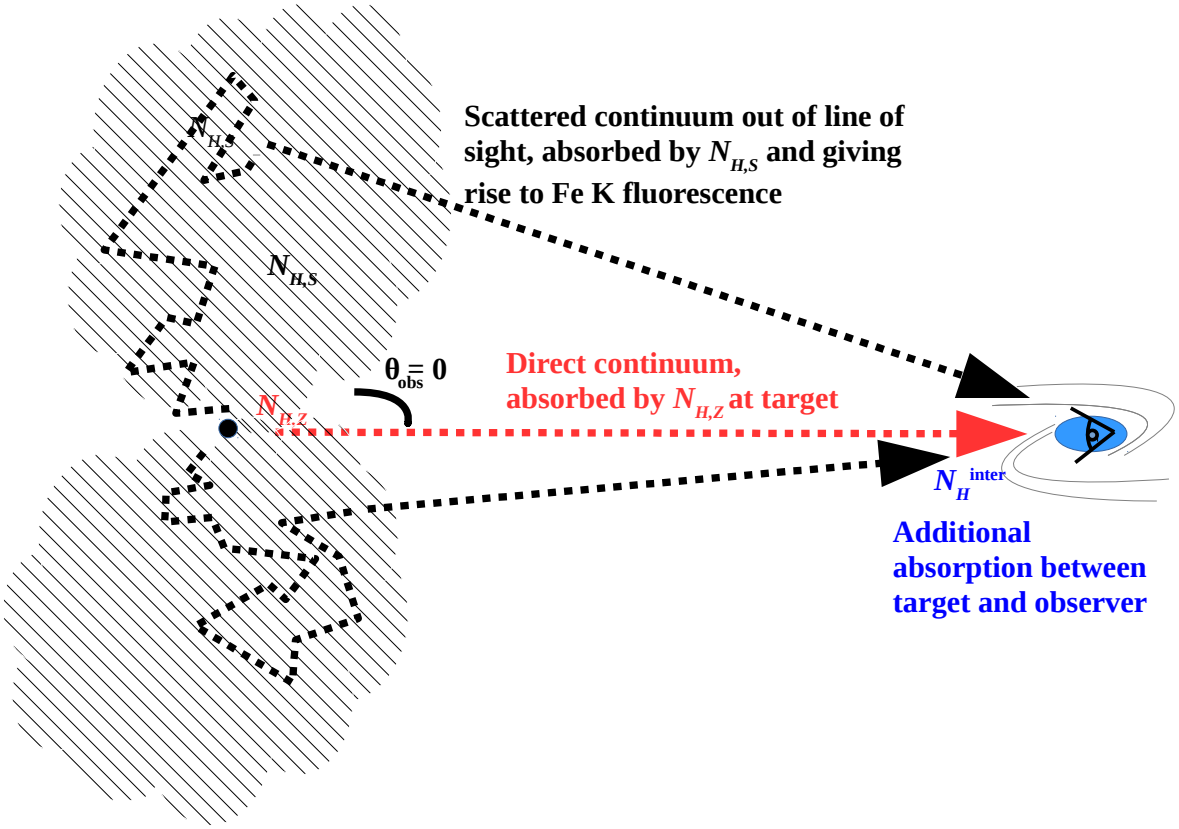

Figure 2: Geometry assumed in decoupled MYTORUS. Part of the intrinsic continuum experiences no Compton scattering and reaches the observer along the line of sight, in the process being attenuated by an equivalent hydrogen column density $N_{\rm H,Z}$ ("direct" or "zeroth" or line-of-sight continuum). Another part of the intrinsic continuum experiences Compton scattering out of the line of sight, and is absorbed by a column density $N_{\rm H,S}$, which also gives rise to the Fe Kα and Kβ fluorescent line emission. Since $N_{\rm H,S}$ is associated with any location out of the line of sight, it is a "global" property. A cross section of the putative torus is drawn in the plane of the page and is for illustration only. In reality in this processing *no torus is assumed* and X-ray reprocessing may occur in a collection of clouds or clumps. Credit: Tzanavaris et al. (2019, Fig. 1), © AAS. Reproduced with permission.

Table 1: Galactic XRB sample for this work. HMXBs are highlighted by red frames. The type of accretor can be either neutron star (NS) or black hole (BH). See text for details. Observation IDs (ObsID) are given in the second column for each object and labeled (Lb.)in the third column for convenience. Credit: Tzanavaris and Yaqoob (2018, Table 1), © AAS. Reproduced with permission.

Source	ObsID	Lb.	Type
4U 1700-37	657	A	HMXB/NS?
4U 1822-371	671	A	LMXB/NS
4U 1822-371	9076	B	LMXB/NS
4U 1822-371	9858	C	LMXB/NS
4U 1908+075	5476	A	HMXB/NS
4U 1908+075	5477	B	HMXB/NS
4U 1908+075	6336	C	HMXB/NS
Cen X-3	1943	A	HMXB/NS
Cen X-3	705	B	HMXB/NS
Cen X-3	7511	C	HMXB/NS
Cir X-1	12235	A	LMXB/NS
Cir X-1	1905	B	LMXB/NS
Cir X-1	1906	C	LMXB/NS
Cir X-1	1907	D	LMXB/NS
Cir X-1	8993	G	LMXB/NS
Cyg X-1	11044	A	HMXB/BH
Cyg X-1	12313	B	HMXB/BH
Cyg X-1	12314	C	HMXB/BH
Cyg X-1	12472	D	HMXB/BH
Cyg X-1	13219	E	HMXB/BH
Cyg X-1	1511	F	HMXB/BH
Cyg X-1	2415	G	HMXB/BH
Cyg X-1	2741	H	HMXB/BH
Cyg X-1	2742	I	HMXB/BH
Cyg X-1	2743	J	HMXB/BH
Cyg X-1	3407	K	HMXB/BH
Cyg X-1	3814	M	HMXB/BH
Cyg X-1	8525	N	HMXB/BH
Cyg X-1	9847	O	HMXB/BH
Cyg X-1	3815	P	HMXB/BH
Cyg X-3	101	A	HMXB/?
γ Cas	1895	A	HMXB/NS
GX 301-2	2733	B	HMXB/NS
GX 301-2	3433	C	HMXB/NS
GX 1+4	2710	A	LMXB/NS
GX 1+4	2744	B	LMXB/NS
Her X-1	2703	A	LMXB/NS
Her X-1	2704	B	LMXB/NS
Her X-1	2705	C	LMXB/NS
Her X-1	2749	D	LMXB/NS
Her X-1	3821	E	LMXB/NS
Her X-1	3822	F	LMXB/NS
Her X-1	4375	G	LMXB/NS
Her X-1	4585	H	LMXB/NS
Her X-1	6149	I	LMXB/NS
Her X-1	6150	J	LMXB/NS
LMC X-4	9571	A	HMXB/NS
LMC X-4	9573	B	HMXB/NS
LMC X-4	9574	C	HMXB/NS
OAO 1657-415	12460	A	HMXB/NS
OAO 1657-415	1947	B	HMXB/NS
Vela X-1	102	A	HMXB/NS
Vela X-1	14654	B	HMXB/NS
Vela X-1	1926	C	HMXB/NS
Vela X-1	1927	D	HMXB/NS
Vela X-1	1928	E	HMXB/NS

4.1. Does HETG spectrally resolve the narrow line in Galactic XRBs?

We find that in about half of the sources the HETG does resolve the narrow line in these systems. This is clear from contour plots of FWHM vs. $N_{\rm H,S}$ for all observations and sources, as illustrated in Figure 3, where in about half of the panels the FWHM part of the contours is bounded.

4.2. What is the geometry of the X-ray reprocessing region?

The main result of this work is that the reprocessing region does not appear to be uniformly spherical. If it were, the uniform spherical reprocessor of the BN11 model, which allows for varying $A_{\rm Fe}$, should fit different observations with the same Fe abundance. However, this happens only for the two observations of GX 301–2, for solar $A_{\rm Fe}$, the single observation of 4U1700–37 for $\sim 0.6 \times$ solar $A_{\rm Fe}$, and three observations of 4U1822–371 for $\sim 3 \times$ solar $A_{\rm Fe}$. For all remaining sources, the best-fit $A_{\rm Fe}$ values vary among observations.

Further, the decoupled MYTORUS model provides good fits for the majority of the observations, suggesting that a solar abundance, clumpy X-ray reprocessor is consistent with the geometry of the distant environment in Galactic XRBs.

4.2.1. Fe K region size

We can use the Fe Kα FWHM values to estimate sizes for the emitting region. If we assume that the reprocessing material is virialized and in Keplerian motion, we can use CO mass values, $M_{\rm CO}$, from the literature to estimate radial distances from the CO via the relation

$$r = \frac{4c^2}{3v^2_{\rm FWHM}} r_g \,,$$

where the gravitational radius $r_g \equiv GM_{\rm CO}/c^2$. G is Newton's gravitational constant and c the speed of light (see Tzanavaris and Yaqoob, 2018, for details). We list ranges of possible minimum and maximum radial distances, corresponding to ranges of $M_{\rm CO}$ values, in Table 2. These ranges suggest distances of the order of about 2×10^{-4} to 3×10^{-3} AU (not considering lower limits).

4.3. What is the Fe abundance of the reprocessing matter?

This question has already been answered above: While a spherical reprocessor appears to require nonsolar Fe abundances in a number of cases, the decoupled MYTORUS results are consistent with solar Fe abundance, which also is the simplest case.

5. Concluding Remarks

This is the first time that two of the most advanced, physically motivated models have been used to model Galactic XRB *Chandra* spectra. We find that the HETG resolves the narrow

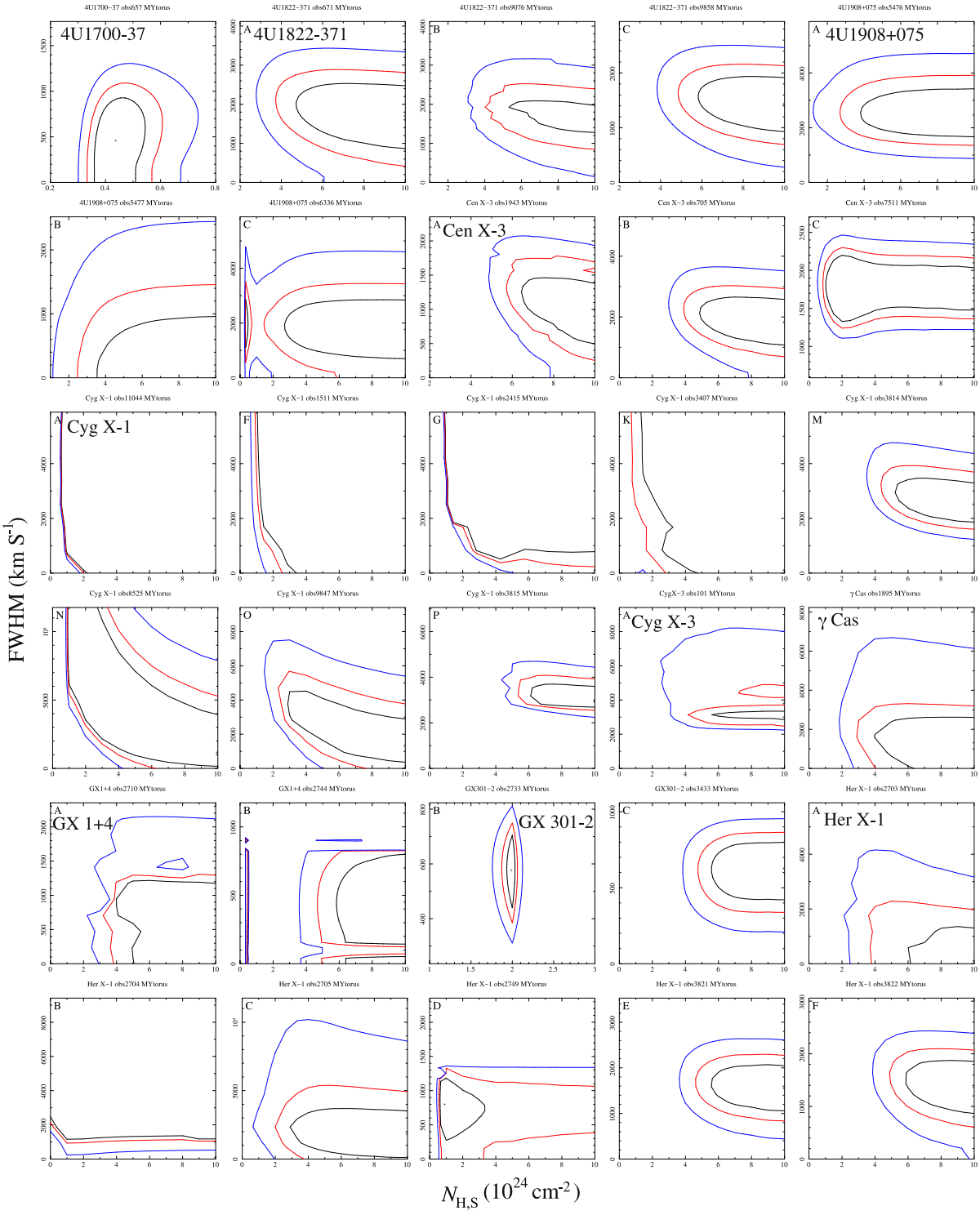

Figure 3: FWHM vs. $N_{\rm H,S}$ contours for a subsample of Galactic XRBs and observations. The contours are for 60%, 90%, and 99% confidence and the decoupled MYTORUS best fits. Closed FWHM contours indicate that the narrow line is resolved. In about half of the panels the FWHM part is bounded. Note that the $N_{\rm H,S}$ part is instead mostly *not* bounded. The lack of high-energy information, such as from the Compton hump, prevents the fits from constraining this parameter. Credit: Tzanavaris and Yaqoob (2018, Fig. 4), © AAS. Reproduced with permission.

Table 2: Estimates for distance ranges of the narrow-line X-ray reprocessing region from the central object. Minimum and maximum distances, $r_{\rm min}$ and $r_{\rm max}$ correspond to maximum and minimum CO masses from the literature. From Tzanavaris and Yaqoob (2018, Table 6), © AAS. Reproduced with permission.

Source	**ObsID**	$r_{\rm min}$ (10^5 km)	$r_{\rm max}$ (10^5 km)
4U 1700-37	657	> 3.651	> 4.545
4U 1822-371	671	$0.596^{+5.738}_{-0.343}$	$1.426^{+13.724}_{-0.821}$
4U 1822-371	9076	$0.646^{+1.363}_{-0.334}$	$1.545^{+3.260}_{-0.798}$
4U 1822-371	9858	$0.837^{+1.461}_{-0.406}$	$2.002^{+3.494}_{-0.972}$
4U 1908+075	5476	$0.410^{+0.758}_{-0.214}$	
4U 1908+075	5477	> 2.200	
4U 1908+075	6336	$0.795^{+4.514}_{-0.503}$	
Cen X-3	1943	$2.192^{+7.715}_{-1.108}$	$2.845^{+10.010}_{-1.438}$
Cen X-3	705	$0.643^{+1.475}_{-0.338}$	$0.835^{+1.914}_{-0.439}$
Cen X-3	7511	$0.698^{+0.300}_{-0.190}$	$0.906^{+0.389}_{-0.246}$
Cyg X-1	3814	$2.846^{+3.876}_{-1.436}$	$4.171^{+5.680}_{-2.104}$
Cyg X-1	9847	> 0.787	> 1.154
Cyg X-1	3815	$2.083^{+1.531}_{-0.830}$	$3.052^{+2.244}_{-1.217}$
Cyg X-3	101	$0.123^{+0.112}_{-0.060}$	$0.982^{+0.896}_{-0.483}$
γ Cas	1895	> 0.087	> 0.415
GX 301-2	2733	$11.578^{+11.995}_{-4.714}$	$20.584^{+21.324}_{-8.381}$
GX 301-2	3433	$8.360^{+11.546}_{-3.459}$	$10.845^{+14.978}_{-4.487}$
GX 1+4	2710	> 1.077	
GX 1+4	2744	> 3.500	
Her X-1	2705	> 0.169	> 0.221
Her X-1	2749	> 1.613	> 2.109
Her X-1	3821	$0.957^{+1.345}_{-0.442}$	$1.251^{+1.759}_{-0.578}$
Her X-1	3822	$1.241^{+2.602}_{-0.603}$	$1.622^{+3.402}_{-0.788}$
Her X-1	4375	$0.132^{+0.296}_{-0.073}$	$0.172^{+0.388}_{-0.095}$
Her X-1	4585	> 0.322	> 0.421
Her X-1	6149	$0.343^{+0.250}_{-0.127}$	$0.448^{+0.327}_{-0.166}$
Her X-1	6150	$1.203^{+3.395}_{-0.636}$	$1.573^{+4.439}_{-0.831}$
LMC X-4	9571	> 0.191	> 0.240
LMC X-4	9573	$0.295^{+0.631}_{-0.153}$	$0.370^{+0.793}_{-0.192}$
OAO 1657-415	12460	> 1.270	> 1.037
OAO 1657-415	1947	> 0.549	> 0.448
Vela X-1	102	> 1.347	> 1.613
Vela X-1	14654	> 3.547	> 4.248
Vela X-1	1927	313.448	375.429
Vela X-1	1928	> 5.034	> 6.029

Fe Kα line in many cases, and that a uniformly spherical X-ray reprocessor is unlikely; at the same time the decoupled MYTORUS model with solar Fe abundance can explain the majority of observations via a clumpy geometry. However, we should note that some of the results are affected by the limited *Chandra* bandpass, thus precluding definitive constraints on parameters such as $N_{\rm H,S}$. Observations spanning longer bandpasses and combining different instruments can help make further progress in this regard.

Acknowledgments

PT thanks the organizers of the LIAC 41 meeting for a stimulating and extremely well-organized meeting, and the American Physical Society for travel support. The material is based upon work supported by NASA under award number 80GSFC21M0002. PT and TY acknowledge support by *Chandra* Award Number AR4-15002A issued by the *Chandra* X-ray Observatory Center.

Further Information

Authors' ORCID identifiers

0000-0001-5737-5055 (Panayiotis TZANAVARIS)

Author contributions

Following the CRediT taxonomy (Contributor Roles Taxonomy), we declare the following contributions for authors.

TY: Conceptualization, funding acquisition, methodology, investigation, formal analysis, data curation.

PT: Formal analysis, investigation, data curation.

Conflicts of interest

The authors declare no conflict of interest.

References

Arnaud, K. A. (1996) XSPEC: The first ten years. In *Astronomical Data Analysis Software and Systems V*, edited by Jacoby, G. H. and Barnes, J., *Astronomical Society of the Pacific Conference Series*, volume 101, pages 17–20. https://www.aspbooks.org/a/volumes/article_details/?paper_id=12588.

Brightman, M. and Nandra, K. (2011) An *XMM–Newton* spectral survey of 12 µm selected galaxies – I. X-ray data. *MNRAS*, **413**(2), 1206–1235. https://doi.org/10.1111/j.1365-2966.2011.18207.x.

Canizares, C., Davis, J., Dewey, D., Flanagan, K., Galton, E., Huenemoerder, D., Ishibashi, K., Markert, T., Marshall, H., McGuirk, M., Schattenburg, M., Schulz, N., Smith, H., and Wise, M. (2005) The *Chandra* high-energy transmission grating: Design, fabrication, ground calibration, and 5 years in flight. *PASP*, **117**(836), 1144–1171. https://doi.org/10.1086/432898.

Murphy, K. D. and Yaqoob, T. (2009) An X-ray spectral model for Compton-thick toroidal reprocessors. *MNRAS*, **397**(3), 1549–1562. https://doi.org/10.1111/j.1365-2966.2009.15025.x.

Torrejón, J. M., Schulz, N. S., Nowak, M. A., and Kallman, T. R. (2010) A *Chandra* survey of fluorescence Fe lines in X-ray binaries at high resolution. *ApJ*, **715**(2), 947–958. https://doi.org/10.1088/0004-637X/715/2/947.

Tzanavaris, P. and Yaqoob, T. (2018) New constraints on the geometry and kinematics of matter surrounding the accretion flow in X-ray binaries from *Chandra* high-energy transmission grating X-ray spectroscopy. *ApJ*, **855**(1), 25. https://doi.org/10.3847/1538-4357/aaaab6.

Tzanavaris, P., Yaqoob, T., LaMassa, S., Yukita, M., and Ptak, A. (2019) Broadband X-ray constraints on the accreting black hole in quasar 4C 74.26. *ApJ*, **885**(1), 62. https://doi.org/10.3847/1538-4357/ab4282.

Yaqoob, T. (2012) The nature of the Compton-thick X-ray reprocessor in NGC 4945: Compton-thick X-ray reprocessor in NGC 4945. *MNRAS*, **423**(4), 3360–3396. https://doi.org/10.1111/j.1365-2966.2012.21129.x.